RSC Advances

ROYAL SOCIETY OF CHEMISTRY

www.rsc.org/advances
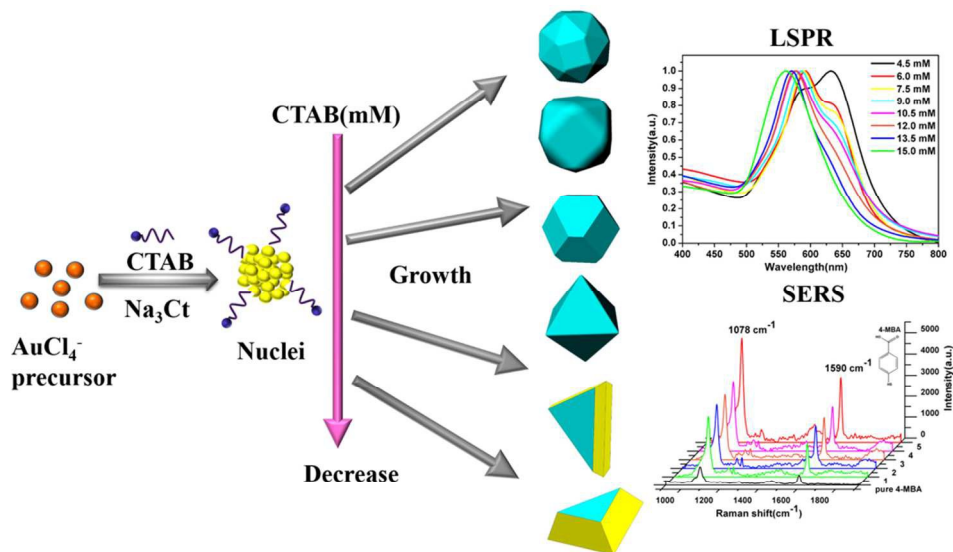
Polyhedral gold nanocrystals with distinctive geometric-dependent plasmonic properties were prepared through hydrothermal strategy.

192x128mm (150 x 150 DPI)

ARTICLE TYPE

Hydrothermal Synthesis of Gold Polyhedral Nanocrystals by Varying Surfactant Concentration and Their LSPR and SERS Properties

Yanting Liu,[a] Jun Zhou,*[a] Xiaocong Yuan,[b] Tao Jiang,[a] Lucia Petti,[c] Lu Zhou ,[a] and Pasquale Mormile[c]

Several polyhedral gold nanocrystals (Au NCs) whose geometric morphology belonging to Platonic solid and Archimedean solid groups are synthesized by modulating cetyltrimethylammonium bromide (CTAB) concentration in the designed hydrothermal processes. The mechanism of growth of these polyhedral Au NCs is revealed via the crystallographic analyses, which suggests that their morphologies mainly depend
10 on the diminishing of the surface energy of the specific facets in the CTAB-directive shape-control process. Furthermore, the localized surface plasmon resonance (LSPR) properties of the as-prepared polyhedral Au NCs are numerically assessed with the finite element method (FEM). The calculations show that these polyhedral Au NCs exhibit the geometry-dependence plasmonic properties: specifically, the enormous local field enhancements occur around their vertices and corner. And the SERS spectra of
15 4-mercaptobenzoic acid molecules adsorbed on these polyhedral Au NCs display the superior SERS activity with the enhancement factor 10^5~10^6 at the excitation wavelength of 785nm. Particularly, the truncated tetrahedron and bitetrahedron show higher SERS enhancement factor due to that their LSPR is closer to the excitation wavelength of 785-nm. Thus, the facile surfactant-assisted synthesis offers the opportunity to design and optimize the shape-dependent SERS activity of polyhedral Au NCs respecting
20 to the possible applications in bio-sensing and imaging.

1. Introduction

Noble metal nanocrystals (NCs) have attracted enormous attention and widespread research interest due to their unique
25 chemical and physical properties and potential applications. [1-6] Especially, the localized surface plasmon resonance (LSPR) property is one of the current prevalent issues, owing to the intriguing optical characteristics arising from the collective oscillation of electrons in the conduction band of metal upon
30 laser irradiation which leads to electromagnetic field enhancement in several orders of magnitude.[3, 7, 8] As the most famous practical consequence of the plasmonic coupling effect,[9] the surface enhanced Raman scattering (SERS) technology has been implemented in ultra-sensitive detections,[10-13] because it can
35 amplify the spectroscopic signatures and offer structural information of target molecules adsorbed on the surface of metal nanostructures.[14, 15] As well known, the LSPR of noble metal NCs exhibits strong dependence on their size, shape and chemical composition. [3, 16] Naturally, the SERS activity of noble metal
40 NCs is highly relying upon their geometry, such as intrinsic enhancement of the local surface plasmon "hot spots" which generate from huge electric field at large curvatures of surfaces.[17] Consequently, it is significant to design and prepare the noble metal NCs with excellent controlled morphology for achieving
45 stronger electric field enhancement and SERS efficiency.[18, 19]

Recently, great efforts have been made to search for the method of fabricating a multiplicity of geometric structures of noble metal NCs, [20-22] such as cube[23], triangular[24], prism[25], sphere[26] and rod[26]. Among them, the isotropic shaped NCs have
50 been systematically studied by many research groups,[20] and the extensive studies are moving the focus towards to anisotropic structures.[16, 27, 28] For example, the synthesis of complicated polyhedral NCs,[29-35] including Platonic solids[36] (tetrahedron, cube, octahedron, dodecahedron, and icosahedron) and Archimedean
55 solids[26] (cuboctahedron, truncated cuboctahedron, truncated octahedron and truncated tetrahedron).[37-44] These solids are categorized in terms of the ancient Greek scientists and very mathematical aesthetics and symmetry in geometry.[45] Various synthetic strategies such as polyol reduction[38], plasmon[46]and
60 photon driven synthesis[47] and seed-assisted growth[1] have been used to achieve the geometry-control of polyhedral Au NCs with the aim to deliberately tailor their plasmonic characteristics.[48] However, the above synthesis routes need the multi-step and intricate rinsing process, or assisted extra-medium. It is often
65 desirable to realize convenient morphological control of Au NCs with simple synthetic progress in water-soluble environment. [49]

In this paper, we report a facile hydrothermal method for synthesizing colloidal Au NCs of diverse geometric features using CTAB as a structure-directing agent. By varying the molar
70 ratio between CTAB and Au precursor, the morphology of Au

NCs can be adjusted from high degree polygons, cuboctahedron, and octahedron to truncated tetrahedron and bitetrahedron, while their LSPR bands continually change from 561 to 627 nm. And the critical role of CTAB in synthetic process has been investigated in the formation of polyhedral Au NCs. In addition, by means of the finite element method (FEM) calculation and Raman measurement, the plasmonic behaviours of these polyhedral Au NCs such as their geometry-dependence electric field enhancement and SERS activities are analysed. At the incident laser of 785 nm, the polyhedral Au NCs have higher SERS efficiencies since the LSPR band approaching to the irradiate wavelength. Overall, this proposed surfactant-assisted synthesize procedure allows us to precisely fabricate the controllable topography of Au NCs and tailor their plasmonic properties for further SERS-based biological applications.

2. Materials and Methods

2.1 Materials

Hydrogen tetrachloroaurate (III) trihydrate ($HAuCl_4 \cdot 3H_2O$) was acquired from Sigma Aldrich. Cetyltrimethylammonium bromide (CTAB) and trisodium citrate ($Na_3C_6H_5O_7 \cdot 2H_2O$) were purchased from Aladdin. 4-Mercaptobenzoic acid (4-MBA) was issued by J&K Chemical. Milli-Q water (18.2 MΩ•cm resistivity) was used for all solution preparations. All chemicals were of analytical grade and used as-received. Glassware were cleaned by aqua regia and rinsed with deionized water several times prior to the experiments.

2.2 Synthesis of polyhedral Au NCs

The synthesis of polyhedral gold nanostructures was accomplished via a modified hydrothermal process.[50] In our work, the different molar ratios of [CTAB]/ [HAuCl$_4$] (CTAB: Au = 15~75) were used to synthesize a diverse of polyhedral Au NCs. In a typical synthesis of the Au high degree polygons, 10 ml of 15mM CTAB, 200 μl of 0.01 M HAuCl$_4$, and 50 μl of 100 mM trisodium citrate aqueous solution were sequentially added and mixed to a 15 ml Teflon-lined stainless-steel autoclave, sealed and then maintained at 110°C for 12 h after the oven had reached this temperature. Then the autoclave was cooled to room temperature naturally. The resulting Au NCs were harvested by centrifugation at 8000 rpm for 20 min and washed with deionized water for another round of centrifugation to remove excess CTAB. Finally the Au NCs were re-dispersed in deionized water for later characterization. The similar procedures were followed to synthesize other Au NCs with different shapes, except that the CTAB concentration was gradually decreased and lead to different molar ratio of CTAB and HAuCl$_4$ in reaction solution, for example, the truncated cuboctahedron (13.5 mM, CTAB /Au = 67.5), cuboctahedron (12.0 mM, CTAB/Au =60), octahedron (10.5 mM, CTAB /Au = 52.5), truncated tetrahedron and bitetrahedron (4.5 mM, CTAB /Au = 22.5).

2.3 Synthesis of 4-MBA-labelled Au NCs

The SERS performances of the as-synthesized polyhedral Au NCs were evaluated with 4-MBA Raman molecules. Firstly, the sample solutions were prepared by respectively adding 20 μl of 1 mM 4-MBA solution to the above purified 5ml of polyhedral Au NCs solutions under stirring, and the resultant solutions were

agitated for 5 h. Afterwards, the mixtures were centrifuged at 10000 rpm for 20 min to remove unbound 4-MBA molecules. Then the sediments at the bottom of centrifuge tubes were re-dispersed in 5 ml deionized water as 4-MBA-labelled polyhedral Au NCs solutions for SERS measurement.

2.4 Instrumentation

UV-Vis absorption spectra were monitored with a spectrometer (TU1901, Pgeneral). SU-70 FESEM instrument was used to record the scanning electron microscopy (SEM) images under an accelerating voltage of 5 kV. Transmission electron microscope (TEM), high-resolution transmission electron microscope (HRTEM) images, selective area electron diffraction (SAED) pattern and energy-dispersive X-ray analysis (EDAX) were obtained with TEM (JEM-2100F, JEOL) operated at accelerating voltage of 200 kV. The SERS properties of the samples were examined by a Raman spectrometer (BWS415, B&W Tek Inc.) using a 785-nm semiconductor laser as the excitation source. Raman spectrographs were recorded with a laser power at the sample position of 49.55 mW and an accumulation time of 10 s. The scattered radiation of the colloid solution and the substrate was collected by a 20×objective lens with numerical aperture (NA) of 0.4 and a 40×objective lens with NA of 0.65, respectively. The wavelength dispersion was performed using a 1200 lines/mm grating, and then passed through a slit with 20 μm width to the charge-coupled device (CCD) (2048×2048 pixels) detector. All the analysis was carried out at room temperature.

2.5 Calculation

The electromagnetic properties of polyhedral Au NCs were numerically simulated by using the commercial FEM software package (COMSOL Mutiphysics 4.4 with the radio frequency module) in an appropriate discrete spatial grid. In our calculations, the frequency dependent dielectric functions for gold are taken from the experimental bulk result of Johnson and Christy.[51] The surrounding medium is presumed to be water with the refractive index 1.33. According to the dimensions extracted from the TEM and SEM images in our experiments, three dimension nanostructure models were constructed to simulate the optical absorption spectra and the distributions of electric near-field intensities of the polyhedral Au NCs.

3. Results and discussion

3.1 Characterization of the polyhedral Au NCs

The morphologies of polyhedral Au NCs synthesized at different CTAB concentrations were analyzed via SEM. Figure 1 presents the SEM images of a diverse of polyhedral Au NCs with uniform in size and shape. It was found that the Au NCs went through a shape evolution by simply diminishing the CTAB concentration from 15 to 4.5 mM. As seen in Fig.1 (a), at a high concentration of CTAB (15.0 mM, CTAB/Au =75), the high degree polygons (quasi-sphere) are obtained with an average size of 82 nm. And the truncated cuboctahedron with an approximate size of 78 nm is observed in Fig. 1 (b) for the concentration of CTAB of 13.5 mM. As decreasing the concentration of CTAB to 12.0 mM, the cuboctahedron as shown in Fig. 1 (c) were produced with a mean size of 74 nm. At the concentration of CTAB of 10.5 mM, the octahedral shaped Au NCs were synthesized with an average size

of 71nm. Upon further decreasing the concentration of CTAB from 9 to 6 mM, we discovered that accompanying with the formation octahedron, a significant proportion of truncated tetrahedron and bitetrahedron were generated as byproduct [50] and
5 their proportion gradually increased as shown in Fig. S1 (ESI†). Eventually, the truncated tetrahedron and bitetrahedron became the dominated products at a lower CTAB concentration of 4.5 mM, which are shown in Fig. 1(e) and 1(f) with average particle sizes of 96 and 92 nm, respectively. In a word, the shapes of
10 these polyhedral Au NCs were evolved from high degree polygons at high concentrations of CTAB, cuboctahedron and octahedron at moderate decreasing concentrations of CTAB to a mixture of truncated tetrahedron and bitetrahedron in the presence of low concentration CTAB.
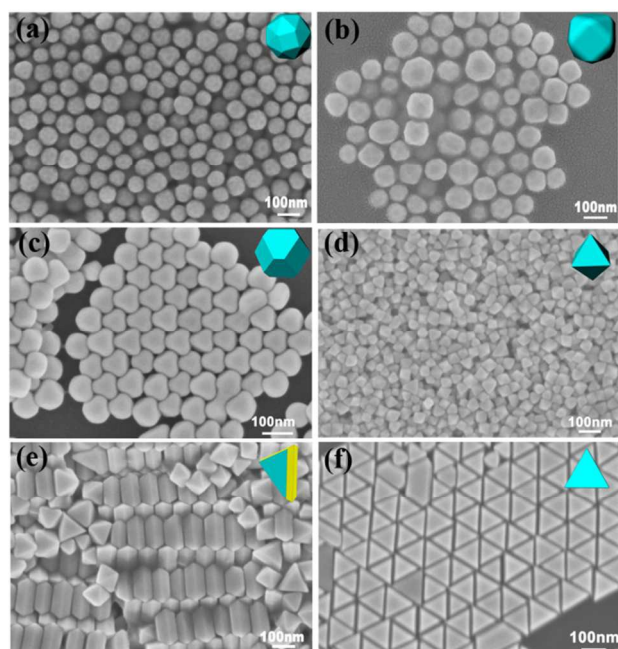

15
Fig. 1 SEM images of the as-synthesized polyhedral Au NCs. (a) high degree polygons, (b) truncated cuboctahedron, (c) cuboctahedron, (d) octahedron, (e) truncated bitetrahedron and (f) truncated tetrahedron. The inset shows the corresponding drawings of the geometric morphology.

20
 Generally, noble metal NCs exhibit very gorgeous color due to the plasmonic property of highly dependent on the crystal size and shape.[16] Fig. 2(a) shows the photograph of colloidal polyhedral Au NCs solutions. The color of solutions gradually
25 changed from blue-gray, purplish, to pink red with CTAB concentration increased. The UV-vis absorption spectra of these polyhedral Au NCs are shown in Fig. 2 (b). With regard to the absorption spectrum of the high degree polygons Au colloid, it shows a LSPR peak at 561 nm, analogous to that of spherical
30 gold nanoparticles with similar size.[23] As decreasing the concentration of CTAB, the LSPR bands of the as-formed Au colloidal solutions display the red-shifts from 571 nm of the truncated cuboctahedron, 574 nm of cuboctahedron to 579 nm of the octahedron. When the CTAB concentration was less than 9
35 mM, however, the LSPR bands of Au colloidal solutions were further red shifts accompanying with raising of shoulders around 625 nm, which is most likely to arise from co-existing triangular particles shown in Fig. S1(ESI†).[24] Eventually, the shoulder was developed into a new LSPR peak at 632 nm at the case of 4.5
40 mM CTAB, which could be attributed to the plasmonic role of

the truncated tetrahedral and bitetrahedral Au NCs. In addition, the relationship of LSPR peak and the concentration of CTAB is plotted as shown in Fig. 2 (c), is clearly demonstrated the shape-dependence LSPR characteristic of Au NCs.
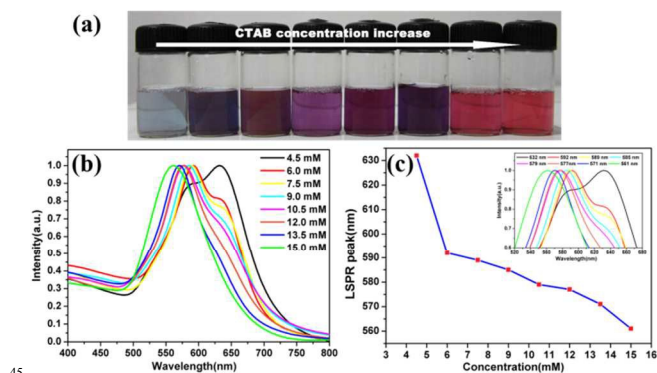

45
Fig. 2 (a) True color pictures and (b) UV-vis absorption spectra of Au NCs colloidal solutions prepared with different concentration of CTAB, and (c) the positions of LSPR peaks corresponding to the concentrations of CTAB, the
50 inset is partial enlargement of absorption spectra.

On the other hand, the crystallography of the as-synthesized polyhedral Au NCs was investigated for providing further insights into the effect of CTAB concentration on the polyhedral structures. Among them, the high degree polygon, the octahedron,
55 the truncated tetrahedron and bitetrahedron were analyzed in details as three typical polyhedral Au structures. Firstly, the high degree polygons are formed under the reacting condition of 15 mM CTAB. The images of SEM and TEM in Fig. 3 (a) and (b) exhibited the polygonal structures are consist of more than 10
60 facets and can also regard as pseudo-spheres with the average diameter of 77±5.0 nm. Figure 3(c) is the corresponding SAED
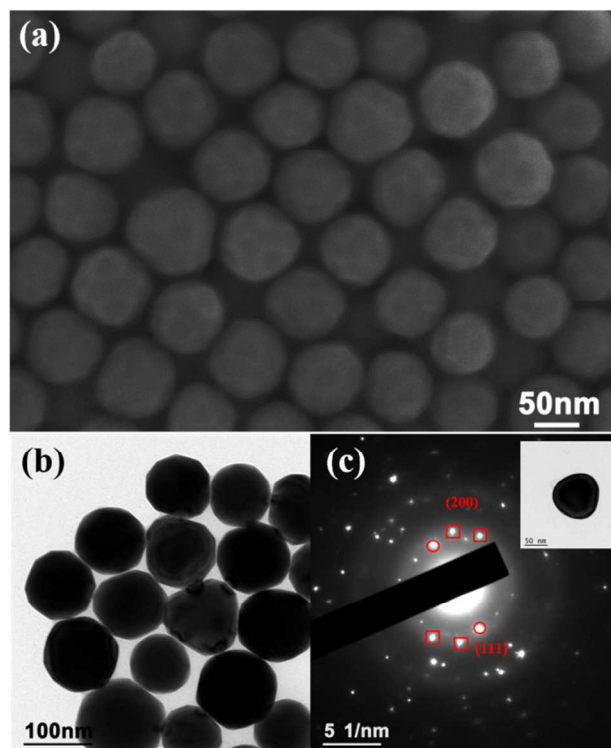

Fig. 3 (a) SEM, (b) TEM images, and (c) corresponding SAED patterns of the
65 high degree polygons. Inset in (c) is HRTEM of an individual high degree polygon.

pattern of individual high degree polygons, which further confirm its single-crystalline structure comprised of two main crystal facets {111} and {100}.[36] Secondly, when the concentration of CTAB is 9 mM, octahedral Au NCs with rounded apexes were mass synthesized. Figure 4 (a) and (b) give the SEM and TEM images of a large quantity of octahedral Au NCs with an average edge length 46±3 nm. Based on simulation of FEM, the optical spectra in Fig. 4 (c) well display the uniform in size of the octahedral Au NC due to the theoretical calculation is almost in accordance with experimental measure. The HRTEM image of a single octahedral Au NC and its corresponding SAED pattern along the [111] zone axis are shown in Fig. 4(d) and (e) respectively. Because the pattern was recorded by focusing the electron beam on one of the triangle faces of an Au octahedron, the SAED spots with the hexagonal symmetry was indexed to {220} reflections, revealing that octahedral Au NC is a single crystal with the {111} facets as the exposed surfaces.[37]
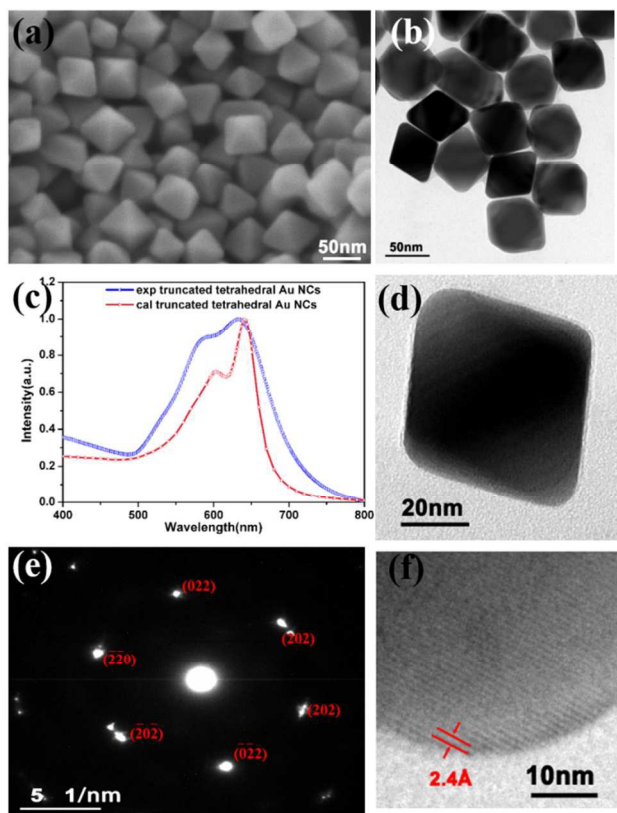
Fig. 4 (a) SEM and (b) TEM images of octahedral Au NCs; (d) HRTEM image, (e) the corresponding SAED pattern along the [111] zone axis and (f) the partial enlarged HRTEM image of a single Au the octahedron; (c) the optical spectra of the octahedrons.

And, Fig. 4 (f) further indicates a lattice spacing of 2.4 Å indexing to {111} planes of the face-centered cubic (fcc) gold according to the JCPDS no.87-0720.[50] Thirdly, as decreasing of the concentration of CTAB to 4.5 mM, the truncated tetrahedron and bitetrahedron were obtained. As shown in Fig. 5 (a) and (c), the as-synthesized Au NCs are triangular structures and seem like triangular prism, however, the clearly slanted sides of the crystals indicate that rather than being flat prisms, these shapes are more accurately described as the tetrahedron with a truncated corner, or the planar twinned analogue of the single crystalline truncated tetrahedron.[38] The optical spectra of the triangular-like Au NCs were also analyzed by comparing the experimental data with the corresponding theoretical results. As seen in Fig. 5 (b), the

positions of LSPR peaks in two spectra are almost the same. It should be noted that, the calculated spectrum shows two narrow LSPR bands, which are different from the experimental results because of only simulating an individual module.[37] Figure. 5(d) and (e) are the HRTEM image of a single truncated tetrahedral Au NC and its corresponding SAED pattern, which confirms that the surface of the tetrahedron is single-crystalline structure and comprises of the crystal faces {111} and {100}.
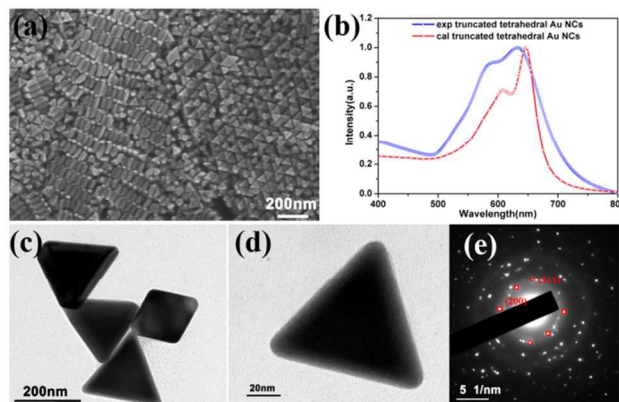

Fig. 5 (a) SEM and (c) TEM images of the truncated tetrahedron and bitetrahedron Au NCs; (d) HRTEM image and (e) the corresponding SAED pattern of a single truncated Au tetrahedron; (b) the optical spectra of the truncated tetrahedron and bitetrahedron.

3.2 Growth Mechanisms of the polyhedral Au NCs

For the growth procedure of the gold nanostructures, many factors such as materials and growth kinetics are considered to be crucial for reaching the final shapes of the resultant NCs.[40, 51, 52] In our synthesis process of the polyhedral Au NCs, the surface-capping agent, reducing agent, temperature and the oxidative etching are believed to play key roles.[2, 31, 38] First of all, from the analysis in section 3.1, it is obvious that the concentrations of CTAB greatly influence the shape and surface structure of the Au NCs. As well known, for the fcc gold crystals, its surface energies of the low-index crystallographic facets are given in the order $\gamma\{111\}<\gamma\{100\}<\gamma\{110\}$, so that the key of shape engineering is able to alter the distribution of exposed crystallographic facets which determine the final shape of nanostructure by promoting selective growth in certain crystallographic directions.[21] Among these three low-index crystallographic facets, {111} facets have a close-packed arrangement of atoms and are the most thermodynamically favoured facets.[48] In the hydrothermal environment, the higher reaction temperature make the thermodynamically stable structures with low-index facets, such as {111}-favour Au NCs, to be easily formed. Considering of our experiment, these fabricated polyhedral Au NCs are mainly consist of the facets {111} and {100}. Therefore, it is believed that CTAB as surfactant is responsible for altering the energy of Au {100} facet relative to others. A systematic shape evolution scheme of the polyhedral Au NCs is illustrated in Fig. 6 from which the synthetic procedure by modulating CTAB concentration can be visualized. Actually, CTAB molecules were represented as micelles in solution and adsorbed on the {100} facets of gold nuclei to lower the energies of {100} facets and slow the growth

of that face for the exposed of the {100} facets.[54] With a high molar ratio of [CTAB]/ [HAuCl$_4$], there is enough micelles to fully coat of the crystal faces of gold nuclei so that the growth takes place on the facets {111} and {100} roughly at the same

behaviour of the as-prepared polyhedral Au NCs, models of the truncated Au octahedral and tetrahedral nanostructures were constructed and their near-field distributions were simulated by FEM. Firstly, for the incident plane-wave polarized along x axis
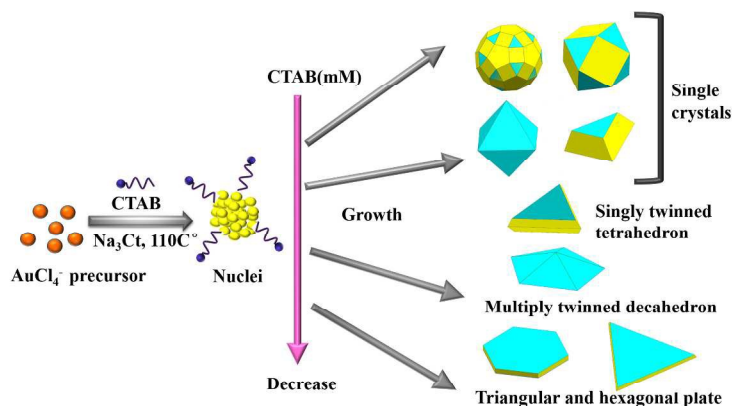

Fig. 6 Schematic of the crystal growth mechanism of polyhedral Au NCs. The blue and yellow colours represent the {111} and {100} facets, respectively.

5 rate.[53] Consequently, the high degree polygons with the bisection mixture of {111} and {100} facets were obtained. Further decreasing molar ratio of CTAB and gold precursor, results in a sequence decrement of {100} facets, thus the {111} facets became the major favour-facet of the Au NCs ranging from 10 cuboctahedron, octahedron with different degree truncation to truncated tetrahedron and bitetrahedron. Progressively, at extremely low molar concentrations of CTAB such as 3 and 1.5 mM, the surface energy of the {100} facets is not able to be declined and the growth is taken along [100] direction to produce 15 the triangular and hexagonal Au nanoplates with a larger area {111} faces shown in Fig. S2 (ESI†).[24]

Besides, the roles of trisodium citrate and oxygen should not be neglected in the process of crystal shape evolution. At our preparing conditions, trisodium citrate is not only used to reduce 20 the gold precursor into Au atoms which further cluster and form into small Au nuclei, [24, 50] but also to promote the formation of {111} facets of nanocrystals and in favour of the growth of nanoplates. Furthermore, as the oxidative etching agent, existing of O$_2$ over the reaction solution could be expected to result in 25 dissolution of Au and completion with the reduction of Au ions, leading to the slow nucleation and the growth of crystals.[35, 42, 51] And the etching effect also caused dissolving of the higher active multiply and twinned crystals while remaining single-crystal particles. [1, 2, 43, 52] After all, by controlling the rate of gold atom 30 added on the crystal surface through synergistic effect of the above discussed factors, the relative growth rates along [100] and [111] directions can be tuned to form particular shapes Au NCs.[3, 27, 29]

3.3 SERS performances of the polyhedral Au NCs.

35 Generally, SERS phenomenon is usually described by two main enhancement mechanisms, the electromagnetic and the chemical enhancement where the former plays the dominating role.[8] As a suitable method, FEM is usually used to numerically analyse the electromagnetic problems of complex metallic nanostructures on 40 an appropriate discretized spatial grid. To pre-estimate the SERS

45 at 785nm wavelength, the enhanced near-field distribution of an individual truncated Au octahedron with the edge length of 45 nm has been calculated as shown in Fig. 7(a), (b) and (c) under the cross-sectional views along x-y, x-z and y-z planes, respectively. As anticipated, the enhanced near-field distribution 50 of octahedron is not uniform across the entire surface of nanostructure, but rather the areas of the most enhanced electric field are located in the vicinities around the tips and edges of the gold octahedron.[9] On the other hand, as shown in Fig. 8, the enhanced near-field distribution of an individual truncated Au 55 tetrahedron with an edge length of 90 nm was analogous to that of the octahedral Au NCs, i.e. the truncated Au tetrahedron generates stronger polarized light-induced electric field located at the edges and corners as well. In addition, the planar twinned analogue of the truncated tetrahedron, a truncated Au 60 bitetrahedron model has also been simulated and the enhanced near-field distributing has shown in Fig. S3 (ESI†). And the high degree polygons can be regard as quasi-spheres, so the enhanced near-field distribution may resemble to that of Au nanospheres with the same dimension was shown in Fig. S4 (ESI†). While
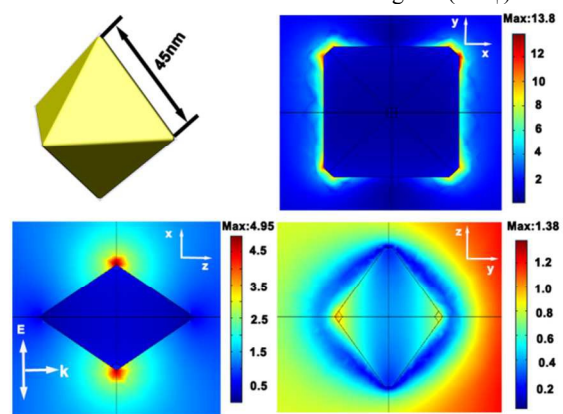

65

Fig. 7 (a) 3D model of the truncated Au octahedron and the corresponding distributions of near-field enhancement in the tangent planes along (a) x-y plane, (b) x-z plane and (c) y-z plane. The coordinate axes and the propagation direction (k vector) and the polarization (E field vector) are shown in white 70 arrows.

comparing with the maximum values of enhanced electric field intensity of the high degree polygons and truncated Au octahedron, the truncated Au tetrahedron and bitetrahedron exhibit stronger electric field enhancements under the excitation light of 785 nm. Next, the SERS performance of the as-prepared polyhedral Au NCs was valued by measuring the Raman spectrum of active molecular 4-MBA with 785-nm semiconductor laser as the excitation source. As shown in Fig. 9, the characteristic fingerprint bands of pure 4-MBA are located at ~1078 and 1590 cm^{-1} which are ascribed to the v (C-C) benzene ring-breathing modes. [55] Especially, for the truncated tetrahedral and bitetrahedral Au NCs synthesized at 4.5 mM CTAB concentration, its SERS signals are the strongest among the 4-MBA labeled polyhedral Au NCs. This is presumably related to the electric near-field enhancement affected by the plasmon resonance behavior of Au NCs. With the formation of triangular analogue structures at a lower concentration of CTAB，the SERS intensity increases as a better resonance coupling between the LSPR peak around 632 nm and the incident laser at 785 nm.[56] The above experimental results are consistent with the enhanced electric near-field intensity calculated by FEM. To see the SERS activities of as-prepared polyhedral Au NCs quantitatively, the enhancement factor (EF) is further estimated by comparing SERS signals with normal Raman intensities obtained from a pure 4-MBA solution. Since the benzene ring C−C stretching mode showed larger intensities, most likely due
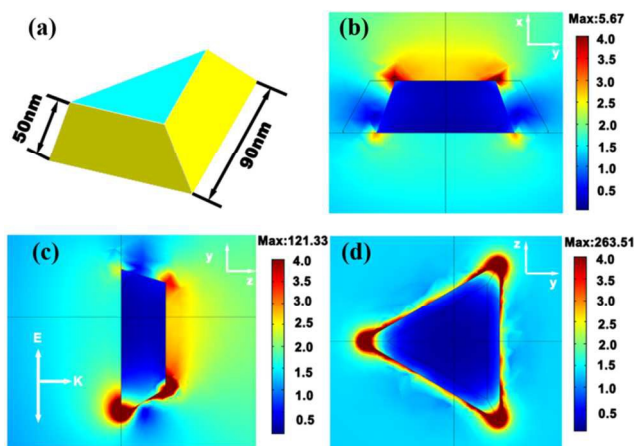
Fig. 8 (a) 3D model of the truncated Au tetrahedron and the corresponding distributions of near-field enhancement in the tangent planes along (a) x-y plane, (b) x-z plane and (c) y-z plane.

to the stronger coupling between the transition dipole moment and the local electric field, the intensity of SERS peak at 1078 cm^{-1} was utilized to calculate the EF value. The calculations are following the equation EF = $(I_{SERS}/I_{bulk}) \times (N_{bulk}/N_{SERS})$, where I_{SERS} and I_{bulk} are the integrated intensities of a characteristic band from SERS and from bulk Raman spectra, respectively; N_{bulk} is the number of bulk molecules probed in the bulk sample; and N_{SERS} is the number of molecules adsorbed on Au NCs. The Raman spectrum of the 4-MBA solution (10 mM) was used to assess the "bulk" values of the EF. The same calculation method has been stated in our previous work, [57] and the detailed numerical calculation process were shown in supporting information (ESI†). Thus, corresponding to the SERS spectra in

Fig. 9, the EF values of the polyhedral Au NCs colloid samples were given as $EF_1 = 7.51 \times 10^5$, $EF_2 = 9.15 \times 10^5$, $EF_3 = 1.01 \times 10^6$, $EF_4 = 1.10 \times 10^6$, $EF_5 = 1.29 \times 10^6$. It reveals all of the polyhedral Au NCs display well SERS activities and the coupling between LSPR and the excitation laser plays an important role in determining SERS enhancement. Therefore, it should be expected that Au polyhedral NCs can serve as superior SERS probes with favorable excitation laser.
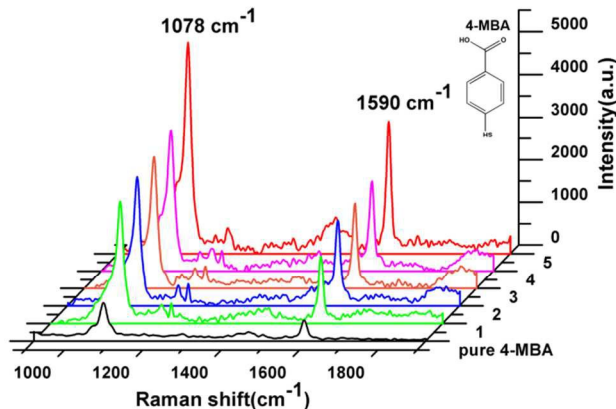
Fig. 9 Raman spectra of 4-MBA labelled polyhedral Au NCs. Labels 1-5 in the y axis correspond to high degree Au polygon, Au truncated cuboctahedron, Au cuboctahedron, Au truncated octahedron and Au truncated bitetrahedron and tetrahedron, respectively.

4. Conclusions

In summary, six classes of well-defined shapes of polyhedral Au NCs have successfully been fabricated through a facile hydrothermal strategy via gradually changing the concentration of CTAB, and the shape-dependent optical properties of these polyhedral Au NCs have systematically been investigated. We have also analyzed elaborately on the formatting mechanism of Au NCs and disclosed that the growth system is {111}-favor Au NCs process. Then the LSPR and the SERS properties were simulated and measured by FEM and 4-MBA molecules adsorbed on the colloidal polyhedral Au NCs, respectively. The results show that SERS enhancement factors have been achieved on the order of $10^5 \sim 10^6$, and the stronger SERS enhancement was observed under near-infrared (785nm) excitation because the laser wavelength approaches the plasmon coupling band of the Au NCs. Therefore, the controllable synthesis of polyhedral Au NCs provides an effective strategy to architecturally design geometry-dependent noble metal materials and tailor their enhancement feature. Furthermore, Au NCs with effective SERS enhancement may lead to potential application such as SERS-based spectroscopy detection of a wide variety of biological molecules.

Notes and references

[a] *Institute of Photonics, Faculty of Science, Ningbo University, Ningbo 31†5211, Zhejiang, China. Tel: +86-574-87600794; Fax: +86-574-87600744; E-mail: zhoujun@nbu.edu.cn*
[b] *Institute of Micro & Nano Optics, Shenzhen University, Shenzhen, 518060, China*
[c] *Institute of Cybernetics "E. Caianiello" of CNR, Via Campi Flegrei 34, 80072 Pozzuoli, Italy*

1   L.Polavarapu, S. Mourdikoudis, I. Pastoriza-Santos and J. Perez-Juste, *CrystEngComm*, 2015, **17**, 3727-3762.
2   Y. Xia, Y. Xiong, B. Lim and S. E. Skrabalak, *Angew. Chem. Int. Ed.*, 2009, **48**, 60-103.
3   C. J. Murphy, T. K. Sau, A. M. Gole, C. J. Orendorff, J. Gao, L. Gou, S. E. Hunyadi and T. Li, *J. Phys. Chem. B*, 2005, **109**, 13857-13870.
4   M. Rycenga, C. M. Cobley, J. Zeng, W. Li, C. H. Moran, Q. Zhang, D. Qin and Y. Xia, *Chem. Rev.*, 2011, **111**, 3669-3712.
5   S. Liu and Z. Tang, *J. Mater. Chem.*, 2010, **20**, 24-35.
6   G. Konstantatos and E. H. Sargent, *Nat Nano*, 2010, 5, 391-400.
7   M. Fernanda Cardinal, B. Rodríguez-González, R. n. A. Alvarez-Puebla, J. Pérez-Juste and L. M. Liz-Marzán, *J. Phys. Chem. C*, 2010, **114**, 10417-10423.
8   J. B. Jackson and N. J. Halas, *Proc. Natl. Acad. Sci.*, 2004, **101**, 17930-17935.
9   D. Lee and S. Yoon, *J. Phys. Chem. C*, 2015, **119**, 7873-7882.
10 G. Zheng, J. Wang, L. Kong, H. Cheng and J. Liu, *Plasmonics*, 2012, **7**, 487-494.
11 Q. Tao, S. Li, C. Ma, K. Liu and Q.-Y. Zhang, *Dalton Trans.*, 2015, 44, 3447-3453.
12 T. Jiang, L. Zhang, H. Jin, X. Wang and J. Zhou, *Dalton Trans.*, 2015, **44**, 7606-7612.
13 C. Farcau, M. Potara, C. Leordean, S. Boca and S. Astilean, *Analyst*, 2013, **138**, 546-552.
14 S. Nie and S. R. Emory, *Science*, 1997, **275**, 1102-1106.
15 J. A. Dieringer, K. L. Wustholz, D. J. Masiello, J. P. Camden, S. L. Kleinman, G. C. Schatz and R. P. Van Duyne, *J. Am. Chem. Soc.*, 2009, **131**, 849-854.
16 E. Hao, G. Schatz and J. Hupp, *J. Fluoresc.*, 2004, **14**, 331-341.
17 J. M. McLellan, A. Siekkinen, J. Chen and Y. Xia, *Chem. Phys. Lett.*, 2006, **427**, 122-126.
18 A. K. Samal, L. Polavarapu, S. Rodal-Cedeira, L. M. Liz-Marzán, J. Pérez-Juste and I. Pastoriza-Santos, *Langmuir*, 2013, **29**, 15076-15082.
19 H.-L. Wu, H.-R. Tsai, Y.-T. Hung, K.-U. Lao, C.-W. Liao, P.-J. Chung, J.-S. Huang, I. C. Chen and M. H. Huang, *Inorg. Chem.*, 2011, **50**, 8106-8111.
20 C. N. R. Rao, H. S. S. Ramakrishna Matte, R. Voggu and A. Govindaraj, *Dalton Trans.*, 2012, **41**, 5089-5120.
21 L. Manna, E. Scher and A. P. Alivisatos, *J. Clust. Sci.*, 2002, **13**, 521-532.
22 Y. Liu, J. Goebl and Y. Yin, *Chem. Soc. Rev.*, 2013, **42**, 2610-2653.
23 H. Wang, C. S. Levin and N. J. Halas, *J. Am. Chem. Soc.*, 2005, **127**, 14992-14993.
24 H.-C. Chu, C.-H. Kuo and M. H. Huang, *Inorg. Chem.*, 2006, **45**, 808-813.
25 C. Xue, J. E. Millstone, S. Li and C. A. Mirkin, *Angew. Chem. Int. Ed.*, 2007, **46**, 8436-8439.
26 S. Zhang, X. Kou, Z. Yang, Q. Shi, G. D. Stucky, L. Sun, J. Wang and C. Yan, *Chem. Commun.*, 2007, **18**, 1816-1818.
27 S. E. Lohse, N. D. Burrows, L. Scarabelli, L. M. Liz-Marzán and C. J. Murphy, *Chem. Mater.*, 2013, **26**, 34-43.
28 T. K. Sau and A. L. Rogach, *Adv. Mater.*, 2010, **22**, 1781-1804.
29 D. Seo, J. C. Park and H. Song, *J. Am. Chem. Soc.*, 2006, **128**, 14863-14870.
30 J. H. Wu, Z. Guan, S. K. Yang, P. Yuan, Q.-H. Xu and G. Q. Xu, *Nanoscale*, 2013, **5**, 2983-2989.
31 T. T. Tran and X. Lu, *J. Phys. Chem. C*, 2011, **115**, 3638-3645.
32 J. Xiao, S. Liu, N. Tian, Z.-Y. Zhou, H.-X. Liu, B.-B. Xu and S.-G. Sun, *J. Am. Chem. Soc.*, 2013, **135**, 18754-18757.
33 Y. Yu, Q. Zhang, X. Lu and J. Y. Lee, *J. Phys. Chem. C*, 2010, **114**, 11119-11126.
34 L. Zhang, W. Niu and G. Xu, *Nano Today*, 2012, 7, 586-605.
35 Q. Fu, Y. Sheng, H. Tang, Z. Zhu, M. Ruan, W. Xu, Y. Zhu and Z. Tang, *ACS Nano*, 2015, **9**, 172-179.
36 F. Kim, S. Connor, H. Song, T. Kuykendall and P. Yang, *Angew. Chem.*, 2004, **116**, 3759-3763.
37 C. Li, K. L. Shuford, Q. H. Park, W. Cai, Y. Li, E. J. Lee and S. O. Cho, *Angew. Chem.*, 2007, 119, 3328-3332.
38 B. Wiley, T. Herricks, Y. Sun and Y. Xia, *Nano Lett.*, 2004, **4**, 1733-1739.
39 H.-L. Wu, C.-H. Kuo and M. H. Huang, *Langmuir*, 2010, **26**, 12307-12313.
40 M. R. Langille, M. L. Personick, J. Zhang and C. A. Mirkin, *J. Am. Chem. Soc.*, 2011, **133**, 10414-10417.
41 C. Cao, S. Park and S. J. Sim, *J. Colloid Interface Sci.*, 2008, **322**, 152-157.
42 W. Niu, S. Zheng, D. Wang, X. Liu, H. Li, S. Han, J. Chen, Z. Tang and G. Xu, *J. Am. Chem. Soc.*, 2009, **131**, 697-703.
43 M. Kim, H. J. Park, S. W. Han, J. Park and W. S. Yun, *B. Korean Chem. Soc.*, 2013, **34**, 2243-2244.
44 P. Zhao, N. Li and D. Astruc, *Coordin. Chem. Rev.*, 2013, **257**, 638-665.
45 P. F. Damasceno, M. Engel and S. C. Glotzer, *Science*, 2012, **337**, 453-457.
46 C. Xue, G. S. Métraux, J. E. Millstone and C. A. Mirkin, *J. Am. Chem. Soc.*, 2008, **130**, 8337-8344.
47 M. R. Langille, M. L. Personick and C. A. Mirkin, *Angew. Chem. Int. Ed.*, 2013, **52**, 13910-13940.
48 R. Contreras-Cáceres, A. Sánchez-Iglesias, M. Karg, I. Pastoriza-Santos, J. Pérez-Juste, J. Pacifico, T. Hellweg, A. Fernández-Barbero and L. M. Liz-Marzán, *Adv. Mater.*, 2008, **20**, 1666-1670.
49 T. Jiang, B. Wang, L. Zhang and J. Zhou, *J. Alloy. Compd.*, 2015, **632**, 140-146.
50 C.-C. Chang, H.-L. Wu, C.-H. Kuo and M. H. Huang, *Chem. Mater.*, 2008, **20**, 7570-7574.
51 P. B. Johnson and R. W. Christy, *Phys. Rev. B*, 1972, **6**, 4370-4379.
52 M. R. Langille, M. L. Personick, J. Zhang and C. A. Mirkin, *J. Am. Chem. Soc.*, 2012, **134**, 14542-14554.
53 M. L. Personick and C. A. Mirkin, *J. Am. Chem. Soc.*, 2013, **135**, 18238-18247.
54 C. Bullen, P. Zijlstra, E. Bakker, M. Gu and C. Raston, *Cryst.Growth & Des.*, 2011, **11**, 3375-3380.
55 A. Michota and J. Bukowska, *J. Raman Spectrosc.*, 2003, **34**, 21-25.
56 Y. Hu, T. Chou, H. Wang and H. Du, *J. Phys. Chem. C*, 2014, **118**, 16011-16018.
57 Y. Liu, J. Zhou, B. Wang, T. Jiang, H.-P. Ho, L. Petti and P. Mormile, *Phys. Chem.Chem. Phys.*, 2015, **17**, 6819-6826.